Annals of Nuclear Energy 144 (2020) 107544

Contents lists available at ScienceDirect

Annals of Nuclear Energy

journal homepage: www.elsevier.com/locate/anucene

Development and verification of heat production and radiation damage energy production cross section module in the nuclear data processing code NECP-Atlas

Wen Yin, Tiejun Zu *, Liangzhi Cao, Hongchun Wu

School of Nuclear Science and Technology, Xi'an Jiaotong University, Xi'an, Shaanxi 710049, China

ARTICLE INFO

Article history:
Received 10 January 2020
Received in revised form 11 April 2020
Accepted 14 April 2020
Available online 3 May 2020

Keywords:
Heating
Radiation damage
DPA
ARC-DPA model
NECP-Atlas

ABSTRACT

The heat production and radiation damage energy production cross section are essential nuclear data to calculate the heating and displacements per atom (DPA) in nuclear material. A new module is developed in nuclear data processing code NECP-Atlas to calculate heat production and radiation damage energy production cross section. Besides of the NRT-DPA model used in the traditional nuclear data processing codes, the state-of-the-art Athermal Recombination Corrected DPA (ARC-DPA) model is also implemented to improve the precision of DPA calculation. ARC-DPA model can be extended from the NRT-DPA model by multiplying the efficiency function. The material constants in the efficiency function can be determined from Molecular Dynamics (MD) simulations or experiments. The material constants of some materials are obtained in this paper. Numerical results show that NECP-Atlas agrees well with NJOY2016 when they use the same models, and the ARC-DPA model implemented in NECP-Atlas improves the precision of DPA calculation.

1. Introduction

Heating is a very important parameter for the nuclear systems. It may represent the product being sold in a power reactor and it may affect the design of peripheral systems such as shields and structural components. Undesirable heating effects will limit the design, and this is particularly true for the plasma facing components in fusion reactor where excessive heating is expected (Farawila et al., 1989). The heating effects of superconducting magnets in fusion systems are also very important. Thus, the accurate calculation of heating in nuclear systems due to the neutrons and photons is a key factor in the design of nuclear systems. The KERMA (Kinetic Energy Release in Materials) factor is necessary for heating calculation.

It is well known that the materials of nuclear systems undergo detrimental changes in their physical and mechanical properties due to exposure to high levels of incident radiations, such as neutrons, gammas and charged particles. Damage to materials caused by neutron irradiation is another important design consideration in fission reactors and is expected to be an even more important problem in fusion power systems. DPA is an important factor used to quantify the level of incident radiations. The radiation damage energy production cross section is the basic data for radiation damage calculation.

Therefore, the nuclear data processing code should provide the KERMA factor and radiation damage energy production cross section for the heating and radiation damage calculations. The early efforts to calculate KERMA factor were started with Ritts et al. (1969). They calculated KERMA factor for some nuclides composing the human body. Abdou and Maynard (1975) made an important contribution in the development of KERMA factor calculation method, and used momentum and energy conservation principle to derive expressions for neutron KERMA factor. This method is called kinematics method. A code, named MACK (Abdou and Maynard (1975)), based on kinematics method to calculate KERMA factors from nuclear data in ENDF format was developed by Abdou. In this code, the energy conservation is also used to check and correct for inconsistencies in basic nuclear data. After that, Farawila (1987) and Zhang and Abdou (1997) introduced further improvements in order to utilize newly available nuclear data in KERMA factor calculations. A code name MAZE was developed by Zhang, and a new KERMA factor library, called MAZE-LIB, for most materials of interest in fusion and other applications was generated. With the introduction of ENDF/B-IV, which contained secondary photon production files for some materials, an alternative method, called energy-balance method (Muir, 1976), became available. With the advent of ENDF/B-VI and later, the spectra of all charged

* Corresponding author.
E-mail address: tiejun@mail.xjtu.edu.cn (T. Zu).

https://doi.org/10.1016/j.anucene.2020.107544
0306-4549/

products including the recoil nucleus for some materials is given. Another method, called direct method, was proposed (Conlin et al., 2016). The nuclear data processing code NJOY (Conlin et al., 2016), which is the widely used nuclear data processing code, contains the module HEATR (MacFarlane et al., 2018) computing neutron KERMA factors using direct method, energy-balance method and kinematics method.

For the calculation of radiation damage energy production cross section, Kinchin and Pease proposed the KP-DPA model (Kinchin and Pease, 1955), based on the kinetics of elastic scattering among hard spheres. The Norgett-Robinson-Torrens (NRT)-DPA model was improved from KP-DPA model in 1975 (Norgett et al., 1975), which is adopted by NJOY to calculate the radiation damage energy production cross section. With the improvement of computational ability and the process of MD simulation, it is found that the NRT-DPA model has several limitations. In particular, the NRT-DPA model overestimates the number of radiation defects produced in energetic cascades in metals (Zinkle and Singh, 1993). Recently, an improved model named ARC-DPA model is proposed by Nordlund et al. (2018), which can provide more physically realistic descriptions of primary defect creation in materials. ARC-DPA model can be extended from the NRT-DPA model by multiplying an efficiency function. The material constants for a given material in the efficiency function can be determined from MD simulations or experiments. However, the material constants are given only for several materials by Nordlund et al. (2018). Though Konobeyev et al. (2017) give material constants for 81 materials by deriving the systematics based on their correlations with various material properties from the observations made in extensive MD simulations and experiments, the DPA results using material constants provided by Konobeyev can't reach high accuracy and are not consistent with that using MD simulations.

NECP-Atlas (Zu et al., 2019) is a nuclear data processing code developed at Xi'an Jiaotong University in China. The motivation for the development is to establish a platform to carry out deeper researches on nuclear data processing method to satisfy the demands on accurate nuclear data in various fields. The heat production and radiation damage energy production cross section module in NECP-Atlas is newly developed to meet the data requirements of nuclear heating and DPA calculations. The accuracy of the module is validated firstly. Besides, in order to realize the more physically realistic DPA calculation, the ARC-DPA model is also used in NECP-Atlas. And the material constants of some materials are obtained by MD simulations in this paper. Detailed DPA calculation and analysis between different DPA models and different evaluated nuclear data libraries are also finished based on different nuclear systems in this paper.

The present paper is organized as follows. The methodologies used in the present work are described in Section 2. In Section 3, the verification of the developed module and newly fitting material constants are given. The analysis and discussion are also given in this section. Some conclusions are given in the last section.

2. Methodologies

2.1. Model for KERMA factor

Heating is a very important parameter for nuclear systems. Nuclear heating can be divided into neutron heating and photon heating. The developed heat production and radiation damage energy production cross section module only calculates the prompt local neutron heating now. Neutron heating at a given location arising from the kinetic energy of the charged products of a neutron induced reaction is proportional to the local neutron flux. The heating rate in a mixture material can be given as:

$$H(E) = \sum_i \sum_j \rho_i k_{ij}(E)\phi(E) \tag{1}$$

where ρ_i is the number density of material i, $k_{ij}(E)$ is the KERMA factor for material i and reaction j at incident energy E, and $\phi(E)$ is the neutron flux at E.

There are three methods used to obtain KERMA factor, namely direct method, energy balance method and kinematics method, respectively.

2.1.1. Direct method

The direct method to calculate KERMA factor is given as follows:

$$k_{ij}(E) = \sum_l \bar{E}_{ijl}(E)\sigma_{ij}(E) \tag{2}$$

where, $\bar{E}_{ijl}(E)$ is the total kinetic energy carried away by the l^{th} species of secondary particles, $\sigma_{ij}(E)$ is the cross section for reaction j of material i at incident energy E, and the sum is carried out over all the charged products of the reaction including the recoil nucleus. If the direct method is adopted, the spectra of all charged particles and recoil nucleus must be given in the ENDF file. Some materials in ENDF/B- VI and later are given the detailed spectral information of all charged particles and recoil nucleus, so the method can be used for these materials in ENDF/B- VI and later.

2.1.2. Energy-balance method

Due to the limitation of direct method that it can only apply to the material with detailed spectral, the energy-balance method is also adopted to calculate KERMA factors in NECP-Atlas apart from the direct method. The energy-balance method guarantees conservation of total energy in large homogeneous systems. The basic principle of energy-balance method is that the energy carried by charged particles is obtained by subtracting the energy allocated to neutrons and photons from the available energy:

$$k_{ij}(E) = \left(E + Q_{ij} - \bar{E}_{ijn} - \bar{E}_{ij\gamma}\right)\sigma_{ij}(E) \tag{3}$$

where$Q_{ij}$is the mass-difference Q-value for material i and reaction j, $\bar{E}_{ijn}$ and $\bar{E}_{ij\gamma}$ are the energy of secondary neutrons and including multiplicity for material i and reaction j, respectively.

This method is well suited for use with the evaluations containing neutron and photon spectral data.

2.1.3. Kinematics method

If the spectra of all charged particles and recoil nucleus are given in the ENDF file, the direct method will be adopted. If the spectra of charged particles or recoil nucleus are not given in the ENDF file, but the spectra of neutron and photon are given, the energy balance method can be used. However, if neither the spectra of recoil nucleus nor photon are given, kinematics method can be used to obtain more accuracy results.

In kinematics method, KERMA factor is calculated by Eq. (2). However, it is different from direct method that the energy of recoil nucleus is calculated using kinematics formula. The kinematics formulations for different reaction type can be found in the report (Kahler et al., 2018).

The relativistic effect is not considered in this paper. It is known that the relativistic effect is become strong with the increase of neutron energy. Some research has been carried out in the relativistic effect on two-body reaction inducing atomic displacement. Chen et al. (2019a) have proved that the relativistic effect is not negligible for incident neutron energy around 200 MeV. Thus, the relativistic effect will be considered in the future work.

2.2. Model for radiation damage energy production cross section

The accuracy of radiation damage energy production cross section, which is the response function for damage energy, is very important for nuclear systems. A large cluster of lattice defects can be produced by the primary recoil nucleus of a nuclear reaction when the recoil nucleus is slowed down in the lattice. Lattice defect is described by DPA. Usually, there are two different methods for DPA calculation when radiation damage energy production cross sections are obtained, i.e. direct and indirect approaches. The direct approach is using neutrons as incident particles and indirect approach is using the primary knock-on atom (PKA) as incident particles. The directly approach is widely used in the nuclear reactor design researches, due to that it can be realized easily using the present transport code. In this approach, the DPA is calculated as follows:

$$DPA = t\int_E \sigma_D(E)\phi(E)dE \tag{4}$$

where t is the neutron irradiation time;$\phi(E)$is the neutron flux;$\sigma_D(E)$is the radiation damage production cross section and it can be transformed from radiation damage energy production cross section$\sigma_{DE}(E)$by:

$$\sigma_D(E) = \frac{0.8\sigma_{DE}(E)}{2E_d} \tag{5}$$

where$E_d$is the angle-averaged threshold energy of atomic displacement;$\sigma_{DE}(E)$can be expressed as:

$$\sigma_{DE}(E) = \sum_i \sigma^i(E)\int_0^{E_R^{\max}} dE_R K^i(E,E_R)E'_a(E_R) \tag{6}$$

where the index i denotes a partial reaction such as (n, n), (n, n′), (n, p), etc.$\sigma^i(E)$is the cross section of reaction i. $K^i(E,E_R)$is kernel of energy transfer from the incident neutron to the recoil nucleus for reaction i.$E'_a(E_R)$is the damage energy when recoil nucleus energy isE_R. For convenience,$E'_a(E_R)$is simplified toE'_a in the following.

The radiation damage energy production cross sections provided by nuclear data processing code are calculated according to Eq. (6). After these data was obtained and the neutron flux was calculated from the neutron transport calculation, the DPA of material can be calculated by Eq. (4) and (5).

The Eq. (4) can be derived from traditional NRT-DPA model or ARC-DPA model. The NRT-DPA model is described in Sec. 2.2.1 and the ARC-DPA model is described in Sec. 2.2.2.

2.2.1. NRT-DPA model

The NRT-DPA model is improved from Kinchin-Pease (KP) model and it can be given by:

$$N(E_a) = \begin{cases} 0, & 0 < E_a < E_d \\ 1, & E_d < E_a < \frac{2E_d}{0.8} \\ \frac{0.8E_a}{2E_d}, & \frac{2E_d}{0.8} < E_a < \infty \end{cases} \tag{7}$$

where$N(E_a)$is the defect number in one reaction;$E_a$is the Lindhard's damage energy (Lindhard et al., 1963);$E_d$is the threshold energy of atomic displacement, and the constant coefficient 0.8 is deduced from the Binary Collision Approximation (BCA) calculations (Robinson and Torrens, 1974). The Lindhard's damage energy is computed with the PKA kinetic energy$E_{PKA}$by:

$$E_a = E_{PKA} \times P(E_{PKA}) \tag{8}$$

where P is the partition function that measures the fraction ofE_{PKA}left in atomic motion and $1 - P$ represents the fraction of energy lost to electronic excitation (Robinson, 1970). The Robinson partition function is used in NRT-DPA model and can be written as:

$$P(E_{PKA}) = \frac{1}{1 + F_L(3.4008\varepsilon^{1/6} + 0.40244\varepsilon^{3/4} + \varepsilon)} \tag{9}$$

where$F_L = 0.133745Z^{2/3}A^{-1/2}$, $\varepsilon = E_{PKA}/E_L$ with $E_L = 86.931Z^{7/3}$, Z and A are the atomic number and the atomic mass number, respectively. The PKA kinetic energy$E_{PKA}$is calculated in nuclear data processing code by integrating energy-angle distribution of PKA or kinematic method.

The formula of NRT-DPA model gives the calculation of defect number in one reaction. In order to obtain the total defect number in the material undergo certain irradiation, the Eq. (7) will be integrated and converted to Eq. (4). According to Eq. (7), theE'_ain Eq. (6) can calculate by:

$$E'_a = \begin{cases} 0, & 0 < E_a < E_d \\ \frac{2E_d}{0.8}, & E_d < E_a < \frac{2E_d}{0.8} \\ E_a, & \frac{2E_d}{0.8} < E_a < \infty \end{cases} \tag{10}$$

The discontinuity of the integrand in Eq. (6) results in the difficulty of numerical convergence of Eq. (6). GLQPI method proposed by Chen and Bernard (2019) can solve this problem very well.

2.2.2. ARC-DPA model

According to the MD simulations and experimental results (Zinkle and Singh, 1993), it is shown that the number of defects that really survive in the irradiated materials is much lower than what is predicted by the NRT model, because the NRT model does not accurately describe the atomic interactions at the thermal spike. The MD simulations of displacement damage cascades in metals have consistently shown closeness to the experimentally observed damage recombination. The results in the work (Nordlund et al., 2018) suggest that the defect production efficiency ξ, which is the ratio of the true number of existing defects to that predicted by NRT model, is much less than 1 for recoil nucleus energy above 1 keV. Thus, the ARC-DPA model is improved from NRT-DPA model and it can be given by:

$$N(E_a) = \begin{cases} 0, & 0 < E_a < E_d \\ 1, & E_d < E_a < \frac{2E_d}{0.8} \\ \frac{0.8E_a}{2E_d}\xi(E_a), & \frac{2E_d}{0.8} < E_a < \infty \end{cases} \tag{11}$$

with the new efficiency function $\xi(E_a)$ given by:

$$\xi(E_a) = \frac{1-c}{(2E_d/0.8)^b}E_a^b + c \tag{12}$$

where b and c are material constants, that need to be determined for a given material from MD simulations or experiments. It is easy to modify computer codes that now use the NRT-DPA model by simply multiplying with the function $\xi(E_a)$.

The only difference between NRT-DPA model and ARC-DPA model is the efficiency function $\xi(E_a)$, so Eq. (4) also can be integrated from Eq. (11). If the ARC-DPA model is adopted, it can be got from Eq. (11) that the E'_a in Eq. (6) should be calculate by:

$$E'_a = \begin{cases} 0, & 0 < E_a < E_d \\ \frac{2E_d}{0.8}, & E_d < E_a < \frac{2E_d}{0.8} \\ E_a\xi(E_a), & \frac{2E_d}{0.8} < E_a < \infty \end{cases} \tag{13}$$

2.2.3. Material constants fitting

Material constants b and c are important parameters for the application of ARC-DPA model. The material constants were given for only eight types of materials when the ARC-DPA model was proposed, and these material constants are given in Table 1. Although material constants were estimated for 70 materials from Li to U using available experimental data by Konobeyev et al. (2017), these material constants are obtained by deriving the sys-

Table 1
Material constants.

Material	Ed (eV)	b	c	Source
Fe	40	−0.568	0.286	Nordlund et al., 2018
Cu	33	−0.68	0.16	Nordlund et al., 2018
Ni	39	−1.01	0.23	Nordlund et al., 2018
Pd	41	−0.88	0.15	Nordlund et al., 2018
Pt	42	−1.12	0.11	Nordlund et al., 2018
W	70	−0.56	0.12	Nordlund et al., 2018
Au	43	−0.789	0.13	Nordlund et al., 2018
Ag	39	−1.063	0.257	Nordlund et al., 2018
Zr	40	−0.57	0.263	This work
Ti	40	−0.222	0.234	This work
Al	27	−0.453	0.481	This work

tematics based on their correlations with various material properties from the observations made in extensive MD simulations and experiments. The accuracy is not very high. Thus, the material constants of some materials are firstly obtained by MD simulations in this paper, including Zr, Ti and Al and then the constants are fixed in NECP-Atlas.

The figure of the defect number versus the kinetic energy of the PKA is shown in Fig. 1. These data obtained by MD simulation is got from Bacon et al. (2000) and Wooding et al. (1998).

It can be concluded from Eq. (11) that the defect number is a function of damage energyE_a. Because the Fig. 1 gives the data of the defect number versus the kinetic energy of the PKA, it needs to change the E_{PKA} into$E_a$by multiplying the partition function shown in Eq. (9). In order to fit the material constants b and c in Eq. (12), the least square method is adopted. The material constants obtained by the fitting method are shown in Table 1. The E_d values of Zr, Ti and Al are from the recommended values in NJOY2016.

3. Numerical results and discussions

In the previous version, NECP-Atlas has comprehensive capabilities of providing cross sections for the deterministic-based and statistics-based transport calculation codes. In order to satisfy the demands on heating and damage data, a new module named Heat_calc has been developed in NECP-Atlas, which is used to generate pointwise heat production cross sections and radiation damage energy production for specified reactions. The new module is validated and used for numerical analysis in this section.

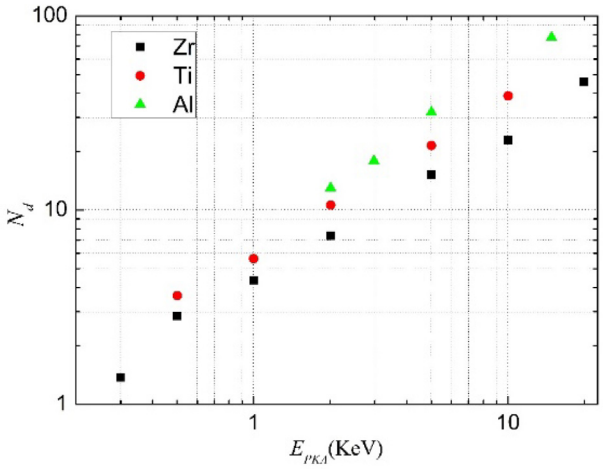

Fig. 1. Log–log plots of *Nd* vs E_{PKA} for Zr, Ti and Al.

3.1. Verification of heat production and radiation damage energy production cross section

NJOY is a widely used and highly accepted nuclear data processing code. In order to verify the newly developed module Heat_calc in NECP-Atlas, the NJOY2016 (Conlin et al., 2016) code is chosen as

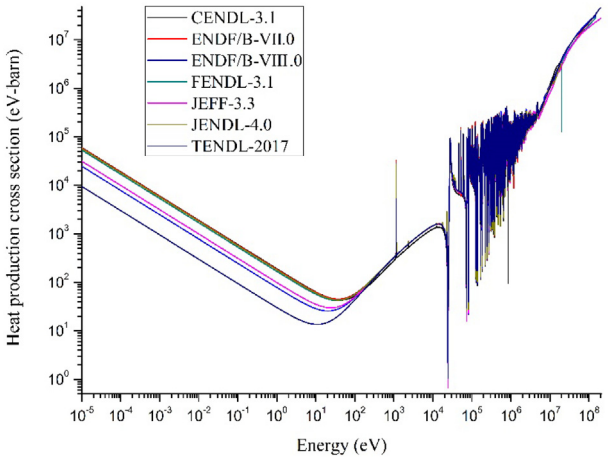

Fig. 2. Heat production cross section of ^{56}Fe.

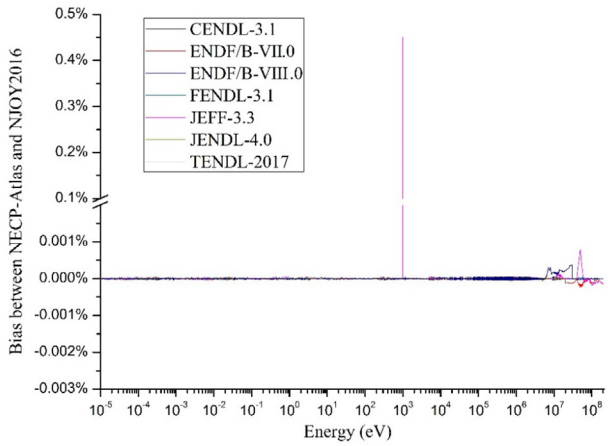

Fig. 3. Bias of heat production cross section for ^{56}Fe.

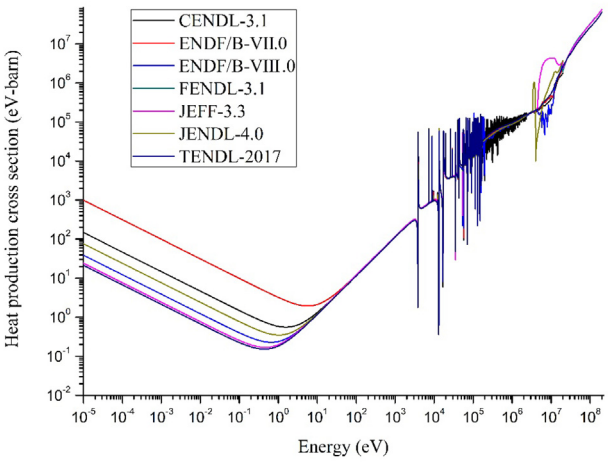

Fig. 4. Heat production cross section of ^{90}Zr.

reference. Due to that NJOY2016 adopts the NRT-DPA model to calculate radiation damage energy production cross section, so we only use it for the verification of the same models in NECP-Atlas. Besides, in order to exclude the influence of other factors, the modules of RECONR and BROADR in NJOY2016 are used to provide the basic cross sections to Heat_calc for the heat production and radiation damage energy production cross section calculations.

3.1.1. Heat production cross section comparison

Fe, Zr, Ti and Al are widely used in the structure or cladding materials of nuclear reactors (Chen et al., 2019b). The heat production cross section of ^{56}Fe, ^{90}Zr, ^{48}Ti and ^{27}Al based on CENDL-3.1, ENDF/B-VII.0, ENDF/B-VIII.0, FENDL-3.1, JEFF-3.3, JENDL-4.0 and TENDL-2017 are analyzed in the present paper.

Figs. 2–9 show the heat production cross sections of ^{56}Fe, ^{90}Zr, ^{48}Ti, ^{27}Al and their bias with NJOY2016. It can be seen that the bias between NECP-Atlas and NJOY2016 is less than 0.001% for all isotopes. For ^{56}Fe, the bias is up to 0.45% in JEFF-3.3 when the neutron energy is 1000 eV, as shown in Fig. 3. The reason is that there are two different photon energy-angle distributions for capture reaction, which is stored as MT102 in MF6 of JEFF-3.3. This is a problem in the JEFF-3.3 library. Due to different algorithm between NECP-Atlas and NJOY2016, it leads NECP-Atlas and NJOY2016 to choose different photon energy-angle distributions in ENDF to calculate photon energy. Thus, the bias becomes larger in JEFF-3.3. Besides, it can also be seen that different evaluated nuclear data libraries have large effect on the heat production cross sections. The reason for this is as follows. Firstly, different evaluated nuclear data libraries store the energy and angle distribution for the secondary particles of a reaction in different MF. In the nuclear data processing code, different calculation methods are used for different MF. Usually, the direct method is used for the reaction types whose products are stored in MF6 and the energy balance method is used for the reaction types whose products are stored in MF4 and MF5. Secondly, even for the reaction types whose products are described by the same MF, the data of different evaluated nuclear data library are different from each other.

3.1.2. Radiation damage energy production cross section comparison

The radiation damage energy production cross sections of ^{56}Fe, ^{90}Zr, ^{48}Ti, ^{27}Al and their bias with NJOY2016 are given in Figs. 10–17. Like the heat production cross section, the bias between NECP-Atlas and NJOY2016 is also less than 0.001% for all isotopes. For ^{56}Fe, the bias is up to 0.40% in JEFF-3.3 when the neutron energy is 1000 eV. The reason is the same as the bias of heat production cross section of ^{56}Fe at 1000 eV in JEFF-3.3. It is the same as the heat production cross section that the difference between various evaluated nuclear data libraries is also very large. The reason is explained in Sec. 3.1.1.

3.2. Verification of ARC-DPA model

3.2.1. Defects comparison with MD simulation

Material constants, *b* and c, are important parameter for the application of ARC-DPA model. In order to verify the accuracy of the fitting method for material constants in this paper, the number of defects atoms of Zr, Ti and Al calculated by ARC-DPA model is compared with the results of MD simulations. As shown in Fig. 18, the results using ARC-DPA model agree well with the results of MD simulations.

Besides, the number of defects calculated by NRT-model and MD simulation are compared in Fig. 19. It can be seen that the steady vacancies predicted by the NRT-DPA model is greater than that of the MD simulations. This can be explained by the fact that the NRT-DPA model does not accurately describe the atomic interactions at the thermal spike. Since the defect center at the thermal spike has a significant kinetic energy, it contributes to the vacancy recovery, and then results in a significant reduction in the number of vacancies.

In order to analyze the difference between NRT-DPA model and ARC-DPA model, the efficiency functions are plotted in Fig. 20. The efficiency function is calculated by Eq. (12). From the Eq. (7), the number of stable defects in NRT-DPA model follows a linear rela-

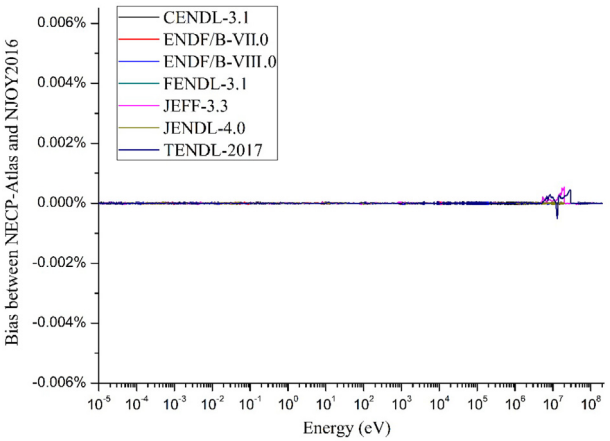

Fig. 5. Bias of heat production cross section for ^{90}Zr.

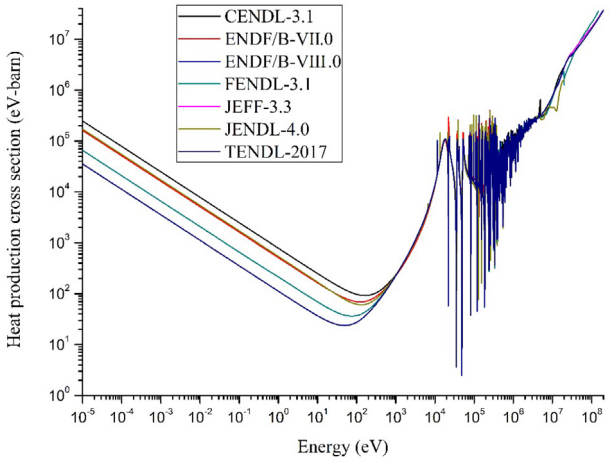

Fig. 6. Heat production cross section of ^{48}Ti.

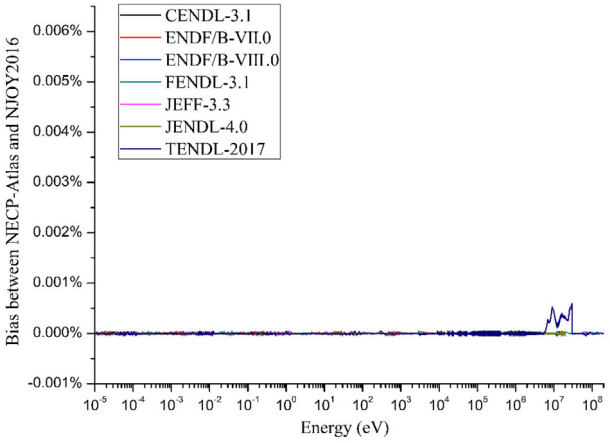

Fig. 7. Bias of heat production cross section for ^{48}Ti.

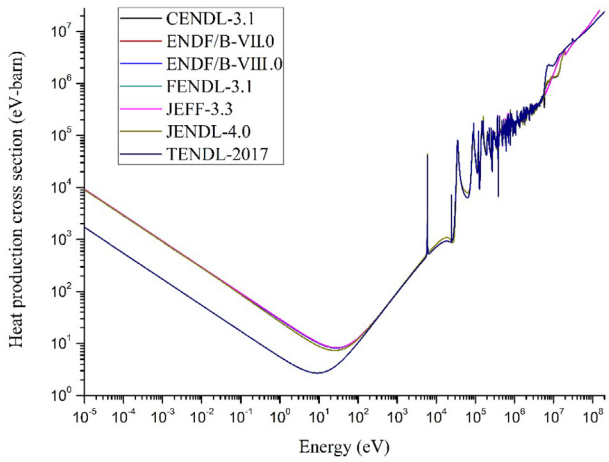

Fig. 8. Heat production cross section of ^{27}Al.

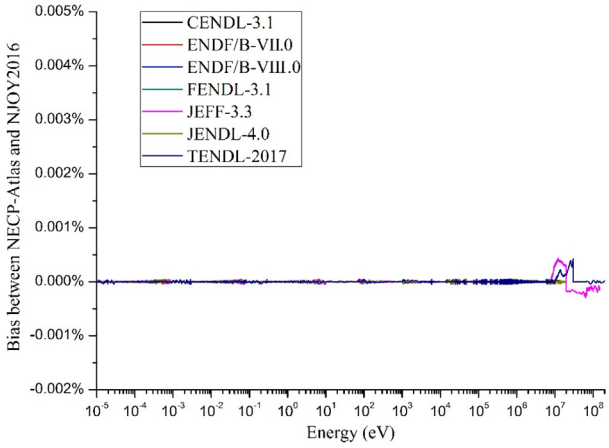

Fig. 9. Bias of heat production cross section for ^{27}Al.

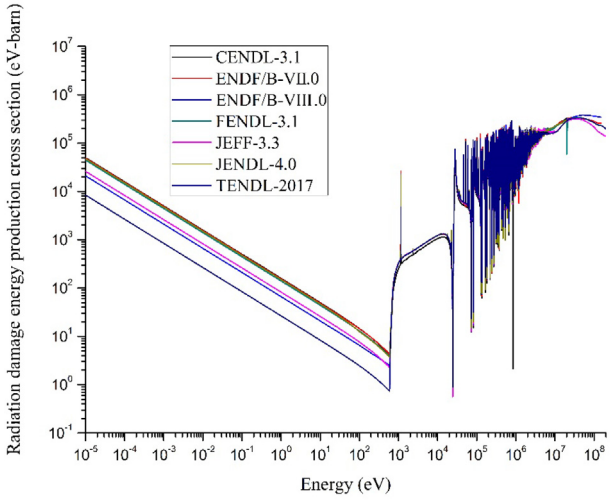

Fig. 10. Radiation damage energy production cross section of ^{56}Fe.

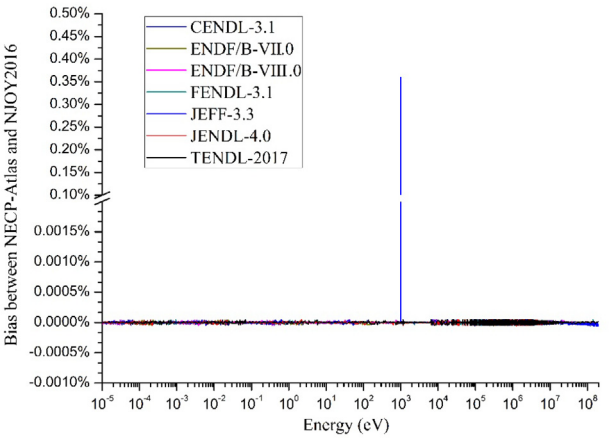

Fig. 11. Bias of radiation damage energy production cross section for ^{56}Fe.

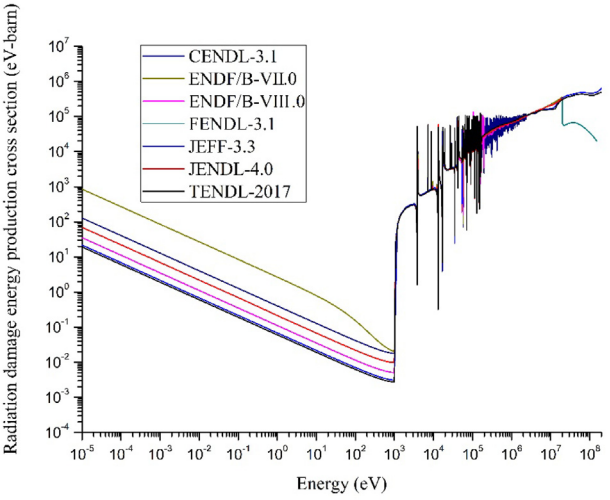

Fig. 12. Radiation damage energy production cross section of ^{90}Zr.

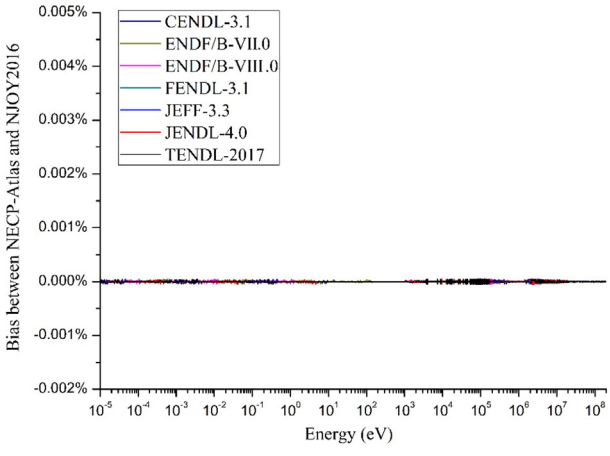

Fig. 13. Bias of radiation damage energy production cross section for ^{90}Zr.

tionship with the damage energy. And it can be known from Eq. (7) and (11) that the efficiency for NRT-DPA model is always equal to 1, because the atomic interactions at the thermal spike are not considered. The efficiency function is also the fraction of remaining defects. As shown in Fig. 20, the fraction of remaining defects is equal to 1, when the damage energy is less than$2E_d/0.8$, and this phenomenon is consistent with NRT-DPA model. However, the efficiency is decreased with damage energy increasing and has a minimum value c when the damage energy is infinite.

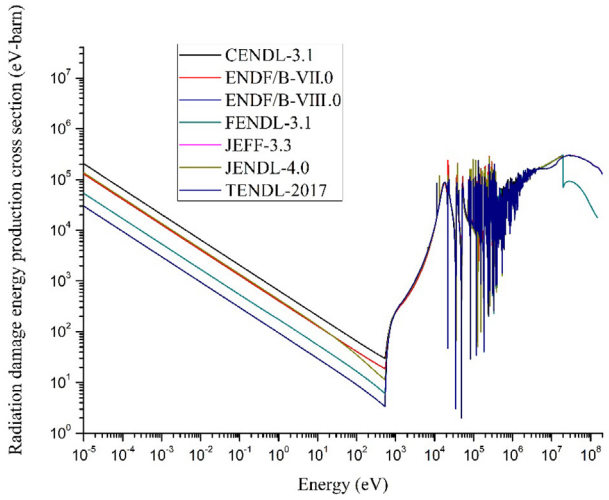

Fig. 14. Radiation damage energy production cross section of ^{48}Ti.

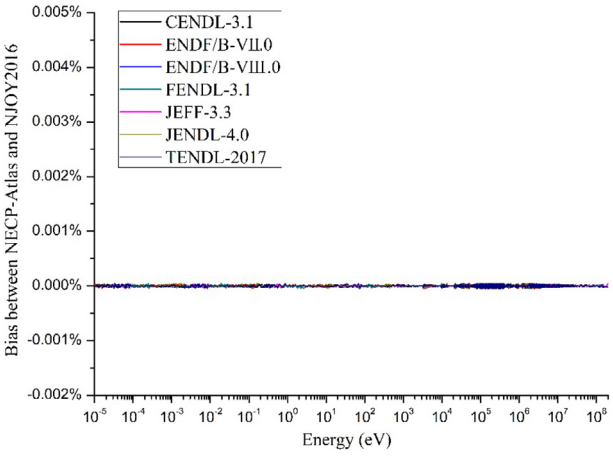

Fig. 15. Bias of radiation damage energy production cross section for ^{48}Ti.

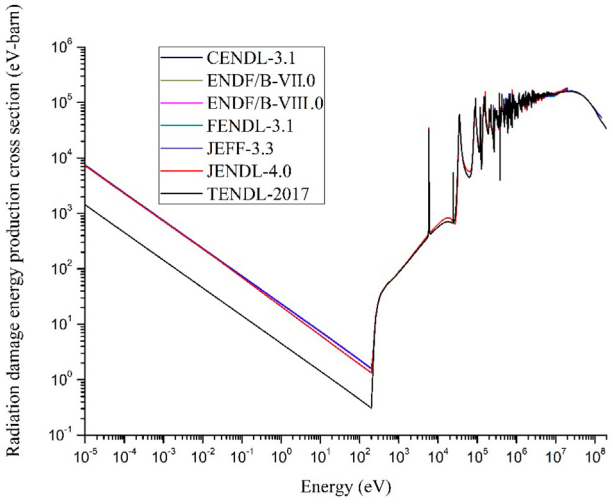

Fig. 16. Radiation damage energy production cross section of ^{27}Al.

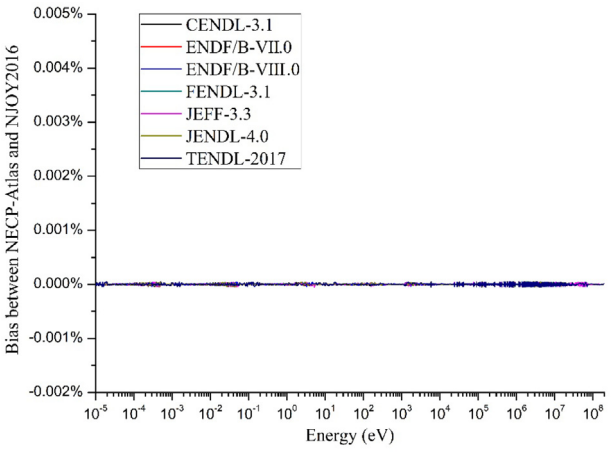

Fig. 17. Bias of radiation damage energy production cross section for ^{27}Al.

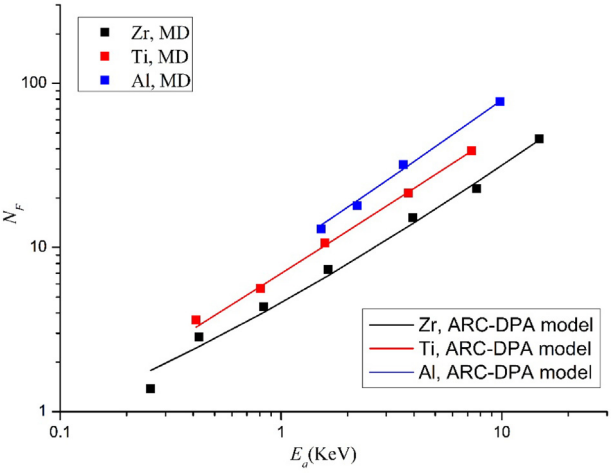

Fig. 18. Number of defects atoms comparison between ARC-model and MD simulation.

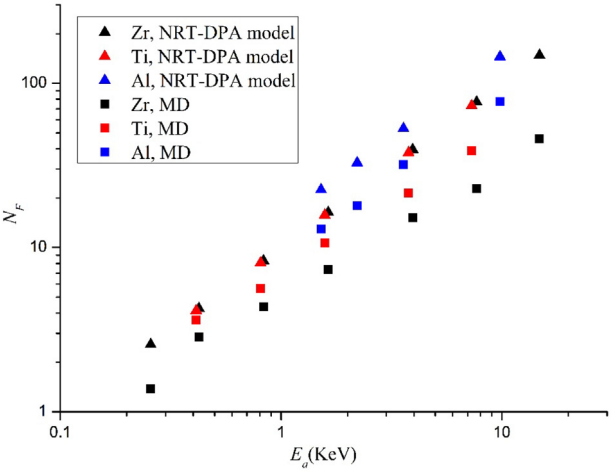

Fig. 19. Number of defects atoms comparison between NRT-model and MD simulation.

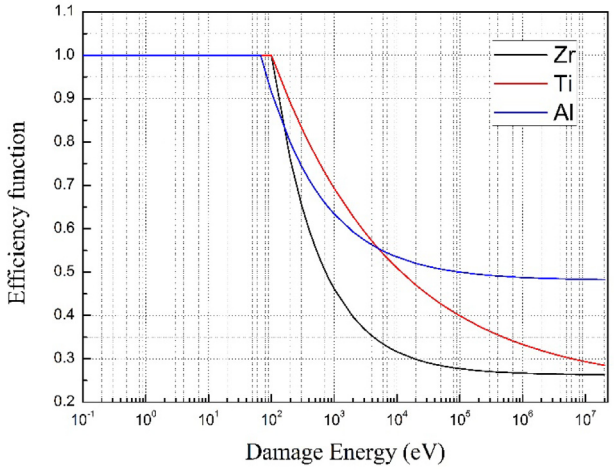

Fig. 20. Efficiency function for Zr, Ti and Al.

3.2.2. Radiation damage energy production cross section comparison between ARC-DPA model and NRT-DPA model

Figs. 21–24 give the radiation damage energy cross section of ^{56}Fe, ^{90}Zr, ^{48}Ti and ^{27}Al produced by NRT-DPA model and ARC-DPA model. In order to explain the impact from different models, only ENDF/B-VIII.0 is selected. It is obvious that the radiation damage energy cross section by ARC-DPA model is much less than that by NRT-DPA model.

3.3. Application of Heat_calc module

3.3.1. Application of heat production cross section

In order to verify the accuracy of heat production cross section, a ^{56}Fe sphere of 50 cm in radius with 20 MeV or 1 keV mono-energy neutron source in the center is assumed and calculated. The model of ^{56}Fe sphere is shown in Fig. 25. Seven types of evaluated nuclear data libraries are used in the calculation. The heating is calculated by continuous-energy Monte Carlo code. The number of histories that were run is 10000000.

Figs. 26 and 27 give the heating results for 20 MeV and 1 keV neutron sources, respectively. The evaluated nuclear data library is ENDF/B-VIII.0. It is obvious that the bias of calculated heating between NECP-Atlas and NJOY2016 is very small whether it is a 20 MeV neutron source or a 1 keV neutron source.

Figs. 28 and 29 give the calculated heating of different evaluated nuclear data libraries. It can be concluded that the deviation of heating calculated by different evaluated nuclear data libraries is very large as the bias of heat production cross section concluded before. As shown in Fig. 28, the bias of different evaluated nuclear data libraries in the model with 20 MeV neutron source is steady. The heating of FENDL-3.1 is larger than others in most region or wider energy range. On the contrary, the heating of JEFF-3.3 is smaller than others in most region or wider energy range. As shown in Fig. 29, the bias of different evaluated nuclear data libraries in the model with 1 keV neutron source is obvious within 10 – 50 cm from center. The reason can be found in Fig. 2, which shows that the bias of heat production cross section is very large between different evaluated nuclear data libraries when neutron energy is less than 500 eV. Because the calculation model is a sphere with mono-energy neutron source, the farther the distance from center, the lower the neutron energy. When neutron reaches 10 cm from center, the energy of the neutron will be lower 500 eV. Thus, the of heating between different evaluated nuclear data libraries will appear in 10 – 50 cm from center.

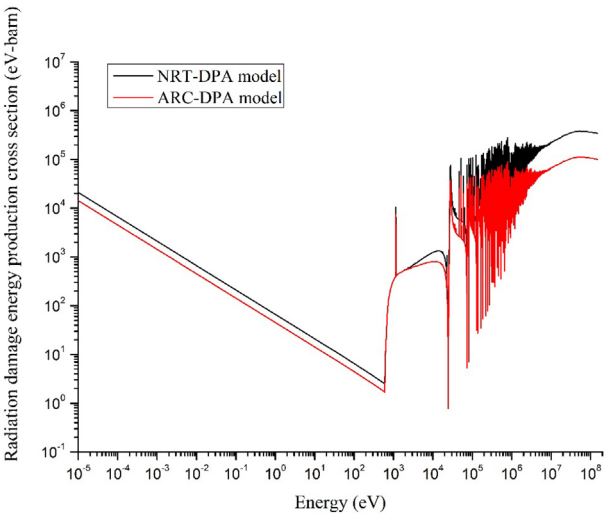

Fig. 21. Radiation damage energy production cross section of ^{56}Fe.

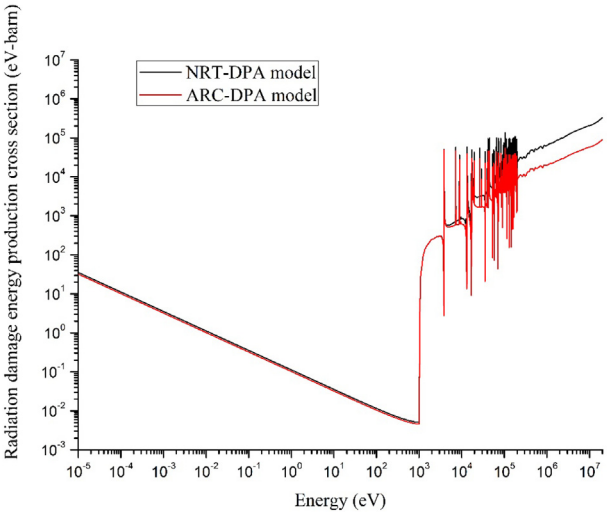

Fig. 22. Radiation damage energy production cross section of ^{90}Zr.

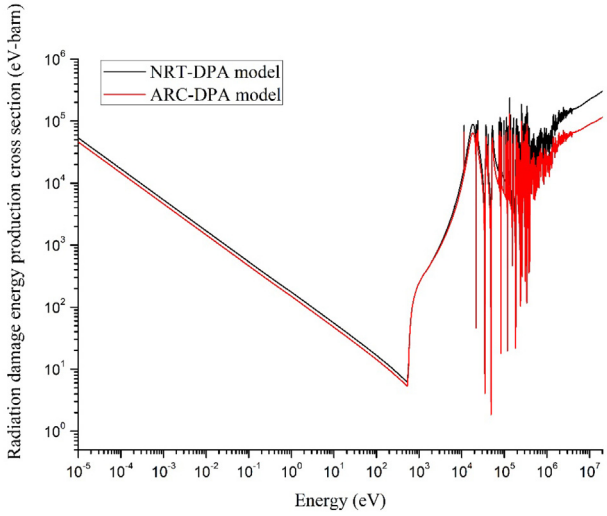

Fig. 23. Radiation damage energy production cross section of ^{48}Ti.

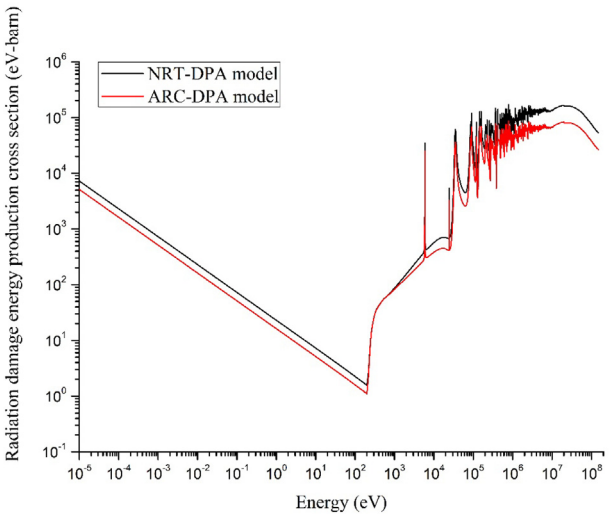

Fig. 24. Radiation damage energy production cross section of ^{27}Al.

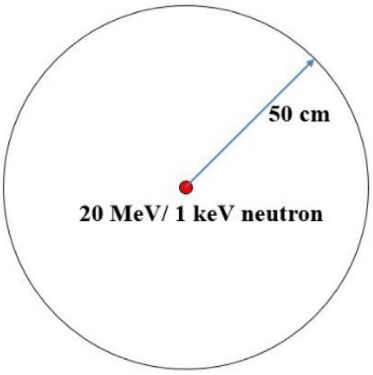

Fig. 25. Model of heating calculation.

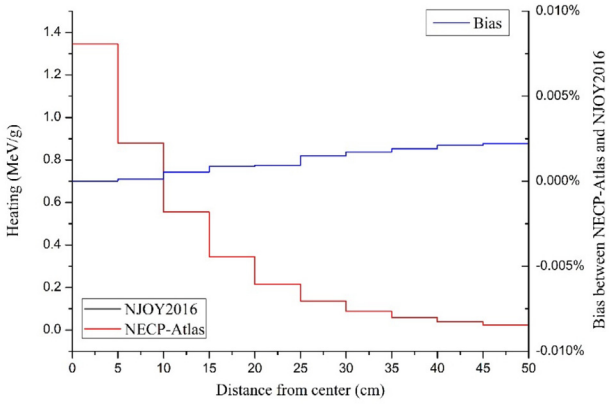

Fig. 26. Calculated nuclear heating and its bias in case of 20 MeV neutron source.

3.3.2. Application of radiation damage energy production cross section

In order to verify the accuracy of radiation damage energy production cross section, the DPA of different nuclear systems are calculated. The different evaluated nuclear data libraries are used in DPA calculation. The nuclear systems include PWR-RPV (Pressurized water reactor, 1/4 Thickness reactor pressure vessel), BWR-RPV (Boiling water reactor, 1/4 Thickness reactor pressure vessel), HCPB-FW (D-T fusion reactor He-cooled pebble bed, first wall) and

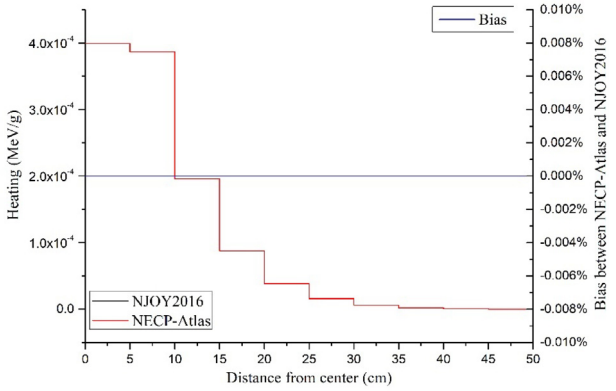

Fig. 27. Calculated nuclear heating and its bias in case of 1 keV neutron source.

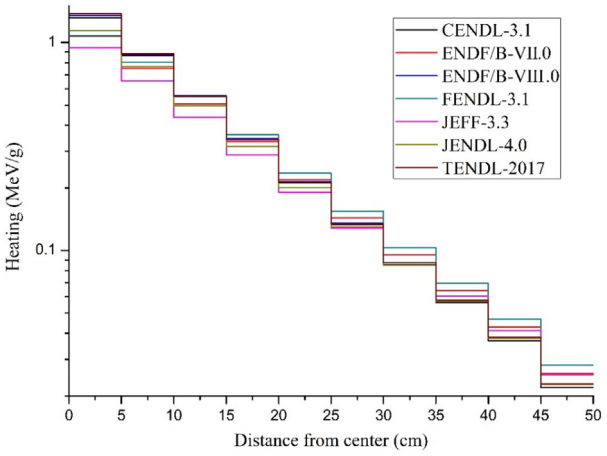

Fig. 28. Calculated nuclear heating of different evaluated nuclear data libraries in case of 20 MeV neutron source.

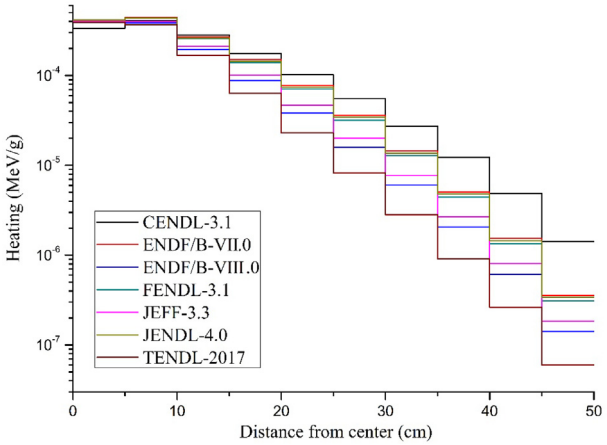

Fig. 29. Calculated nuclear heating of different evaluated nuclear data libraries in case of 1 keV neutron source.

Superphenix (Fast breeder reactor) (Fleming, et al., 2019). The evaluated nuclear data libraries include CENDL-3.1, ENDF/B-VII.0, ENDF/B- VIII.0, FENDL-3.1, JEFF3.3, JENDL-4.0 and TENDL-2017. In order to verify the accuracy of HEAT_calc module in NECP-Atlas, the DPA are calculated using NJOY2016 and NRT-DPA model of NECP-Atlas. To show the impact of ACR-DPA model on DPA, the

Table 2
Total neutron DPA in ^{56}Fe for one EFPY.

ENDF	Code(Model)	Spectrum PWR-RPV	BWR-RPV	HCPB-FW	Superphenix
CENDL-3.1	NJOY2016	1.148E-03	2.078E-04	1.128E + 01	7.705E-15
	NECP-Atlas(NRT)	1.148E-03	2.078E-04	1.128E + 01	7.705E-15
	NECP-Atlas(ARC)	3.692E-04	6.612E-05	3.492E + 00	2.603E-15
ENDF/B- VII.0	NJOY2016	1.166E-03	2.098E-04	1.176E + 01	8.042E-15
	NECP-Atlas(NRT)	1.166E-03	2.098E-04	1.176E + 01	8.042E-15
	NECP-Atlas(ARC)	3.755E-04	6.680E-05	3.640E + 00	2.717E-15
ENDF/B- VIII.0	NJOY2016	1.182E-03	2.121E-04	1.136E + 01	8.119E-15
	NECP-Atlas(NRT)	1.182E-03	2.121E-04	1.136E + 01	8.119E-15
	NECP-Atlas(ARC)	3.801E-04	6.747E-05	3.523E + 00	2.742E-15
FENDL-3.1	NJOY2016	1.142E-03	2.058E-04	1.119E + 01	7.790E-15
	NECP-Atlas(NRT)	1.142E-03	2.058E-04	1.119E + 01	7.790E-15
	NECP-Atlas(ARC)	3.679E-04	6.558E-05	3.470E + 00	2.637E-15
JEFF-3.3	NJOY2016	1.127E-03	2.016E-04	1.002E + 01	7.764E-15
	NECP-Atlas(NRT)	1.127E-03	2.016E-04	1.002E + 01	7.765E-15
	NECP-Atlas(ARC)	3.634E-04	6.427E-05	3.124E + 00	2.629E-15
JENDL-4.0	NJOY2016	1.168E-03	2.094E-04	1.130E + 01	8.062E-15
	NECP-Atlas(NRT)	1.168E-03	2.094E-04	1.130E + 01	8.062E-15
	NECP-Atlas(ARC)	3.764E-04	6.675E-05	3.505E + 00	2.727E-15
TENDL-2017	NJOY2016	1.164E-03	2.060E-04	1.013E + 01	8.143E-15
	NECP-Atlas(NRT)	1.164E-03	2.061E-04	1.013E + 01	8.143E-15
	NECP-Atlas(ARC)	3.755E-04	6.574E-05	3.164E + 00	2.755E-15

Table 3
Total neutron DPA in ^{90}Zr for one EFPY.

ENDF	Code(Model)	Spectrum PWR-RPV	BWR-RPV	HCPB-FW	Superphenix
CENDL-3.1	NJOY2016	1.352E-03	2.315E-04	1.192E + 01	8.629E-15
	NECP-Atlas(NRT)	1.352E-03	2.315E-04	1.192E + 01	8.629E-15
	NECP-Atlas(ARC)	4.261E-04	7.161E-05	3.550E + 00	2.895E-15
ENDF/B- VII.0	NJOY2016	1.400E-03	2.383E-04	1.246E + 01	9.040E-15
	NECP-Atlas(NRT)	1.400E-03	2.383E-04	1.246E + 01	9.040E-15
	NECP-Atlas(ARC)	4.423E-04	7.386E-05	3.706E + 00	3.040E-15
ENDF/B- VIII.0	NJOY2016	1.327E-03	2.279E-04	1.143E + 01	8.408E-15
	NECP-Atlas(NRT)	1.327E-03	2.279E-04	1.143E + 01	8.408E-15
	NECP-Atlas(ARC)	4.193E-04	7.060E-05	3.415E + 00	2.831E-15
FENDL-3.1	NJOY2016	1.354E-03	2.317E-04	1.163E + 01	8.578E-15
	NECP-Atlas(NRT)	1.354E-03	2.317E-04	1.163E + 01	8.578E-15
	NECP-Atlas(ARC)	4.285E-04	7.189E-05	3.476E + 00	2.887E-15
JEFF-3.3	NJOY2016	1.420E-03	2.390E-04	1.082E + 01	9.254E-15
	NECP-Atlas(NRT)	1.420E-03	2.390E-04	1.082E + 01	9.254E-15
	NECP-Atlas(ARC)	4.482E-04	7.411E-05	3.264E + 00	3.101E-15
JENDL-4.0	NJOY2016	1.354E-03	2.317E-04	1.163E + 01	8.578E-15
	NECP-Atlas(NRT)	1.354E-03	2.317E-04	1.163E + 01	8.578E-15
	NECP-Atlas(ARC)	4.285E-04	7.189E-05	3.476E + 00	2.887E-15
TENDL-2017	NJOY2016	1.420E-03	2.384E-04	1.018E + 01	9.188E-15
	NECP-Atlas(NRT)	1.420E-03	2.384E-04	1.018E + 01	9.188E-15
	NECP-Atlas(ARC)	4.483E-04	7.392E-05	3.085E + 00	3.072E-15

DPA using ARC-DPA model of NECP-Atlas is also obtained. The calculated values of DPA in ^{56}Fe, ^{90}Zr, ^{48}Ti and ^{27}Al for one effective full power year (EFPY) of operation in different neutron spectra and different models are presented in Tables 2 – 5. For more intuitive observation, the calculated values of DPA in ^{56}Fe, ^{90}Zr, ^{48}Ti and ^{27}Al for one EFPY of operation in different neutron spectra adopting NRT-DPA model are presented in Figs. 30–33 at the same time.

It can be got from the results of Tables 2 – 5 that the DPA calculated by NRT-DPA model of NECP-Atlas is very close to that calculated by NJOY2016 for different evaluated nuclear data libraries and different nuclear systems. It can be confirmed that the radiation damage energy production cross section produced by NECP-Atlas is correct.

An important conclusion can be got from the results of Tables 2 – 5 that obvious difference in DPA values will happen in different evaluated nuclear data libraries. This phenomenon is especially obvious in HCPB-FW. For example, the DPA value in ^{56}Fe of HCPB-FW using ENDF/B- VII.0 is 11.76, but it is 10.02 when using JEFF-3.3. The bias is about 17%. It should be careful that the bias of DPA value in ^{48}Ti of Superphenix using different evaluated nuclear data libraries and the DPA value calculated by CENDL-3.1 is larger than others obviously.

4. Conclusions

The heat production and radiation damage energy production cross section module named HEAT_calc is newly developed in nuclear data processing code NECP-Atlas to meet the data requirements of nuclear heating and DPA calculation. In the heating production cross section calculation, direct method and energy-balance method are used in NECP-Atlas. In radiation damage energy production cross section calculation, the traditional NRT-DPA model is adopted. In order to realize the more physically real-

Table 4
Total neutron DPA in ^{48}Ti for one EFPY.

ENDF	Code(Model)	Spectrum PWR-RPV	BWR-RPV	HCPB-FW	Superphenix
CENDL-3.1	NJOY2016	1.396E-03	2.418E-04	1.292E + 01	1.156E-14
	NECP-Atlas(NRT)	1.396E-03	2.418E-04	1.292E + 01	1.156E-14
	NECP-Atlas(ARC)	6.686E-04	1.126E-04	5.773E + 00	6.351E-15
ENDF/B- VII.0	NJOY2016	1.309E-03	2.286E-04	1.258E + 01	1.102E-14
	NECP-Atlas(NRT)	1.309E-03	2.286E-04	1.258E + 01	1.102E-14
	NECP-Atlas(ARC)	6.267E-04	1.061E-04	5.626E + 00	6.092E-15
ENDF/B- VIII.0	NJOY2016	1.247E-03	2.203E-04	1.211E + 01	9.820E-15
	NECP-Atlas(NRT)	1.247E-03	2.203E-04	1.211E + 01	9.820E-15
	NECP-Atlas(ARC)	5.936E-04	1.017E-04	5.364E + 00	5.396E-15
FENDL-3.1	NJOY2016	1.247E-03	2.203E-04	1.211E + 01	9.820E-15
	NECP-Atlas(NRT)	1.247E-03	2.203E-04	1.211E + 01	9.820E-15
	NECP-Atlas(ARC)	5.936E-04	1.017E-04	5.364E + 00	5.396E-15
JEFF-3.3	NJOY2016	1.224E-03	2.147E-04	1.084E + 01	9.721E-15
	NECP-Atlas(NRT)	1.224E-03	2.147E-04	1.084E + 01	9.721E-15
	NECP-Atlas(ARC)	5.817E-04	9.898E-05	4.867E + 00	5.340E-15
JENDL-4.0	NJOY2016	1.275E-03	2.244E-04	1.225E + 01	1.007E-14
	NECP-Atlas(NRT)	1.275E-03	2.244E-04	1.225E + 01	1.007E-14
	NECP-Atlas(ARC)	6.061E-04	1.036E-04	5.423E + 00	5.534E-15
TENDL-2017	NJOY2016	1.224E-03	2.147E-04	1.084E + 01	9.720E-15
	NECP-Atlas(NRT)	1.224E-03	2.147E-04	1.084E + 01	9.720E-15
	NECP-Atlas(ARC)	5.815E-04	9.895E-05	4.864E + 00	5.339E-15

Table 5
Total neutron DPA in ^{27}Al for one EFPY.

ENDF	Code(Model)	Spectrum PWR-RPV	BWR-RPV	HCPB-FW	Superphenix
CENDL-3.1	NJOY2016	2.511E-03	4.077E-04	1.612E + 01	1.761E-14
	NECP-Atlas(NRT)	2.511E-03	4.077E-04	1.612E + 01	1.761E-14
	NECP-Atlas(ARC)	1.303E-03	2.106E-04	8.267E + 00	9.290E-15
ENDF/B- VII.0	NJOY2016	2.509E-03	4.078E-04	1.575E + 01	1.774E-14
	NECP-Atlas(NRT)	2.509E-03	4.078E-04	1.575E + 01	1.774E-14
	NECP-Atlas(ARC)	1.301E-03	2.105E-04	8.085E + 00	9.353E-15
ENDF/B- VIII.0	NJOY2016	2.509E-03	4.078E-04	1.575E + 01	1.774E-14
	NECP-Atlas(NRT)	2.509E-03	4.078E-04	1.575E + 01	1.774E-14
	NECP-Atlas(ARC)	1.301E-03	2.105E-04	8.084E + 00	9.353E-15
FENDL-3.1	NJOY2016	2.509E-03	4.078E-04	1.575E + 01	1.774E-14
	NECP-Atlas(NRT)	2.509E-03	4.078E-04	1.575E + 01	1.774E-14
	NECP-Atlas(ARC)	1.301E-03	2.105E-04	8.085E + 00	9.353E-15
JEFF-3.3	NJOY2016	2.514E-03	4.090E-04	1.585E + 01	1.775E-14
	NECP-Atlas(NRT)	2.514E-03	4.090E-04	1.585E + 01	1.775E-14
	NECP-Atlas(ARC)	1.304E-03	2.111E-04	1.585E + 01	9.359E-15
JENDL-4.0	NJOY2016	2.512E-03	4.081E-04	1.615E + 01	1.762E-14
	NECP-Atlas(NRT)	2.512E-03	4.081E-04	1.615E + 01	1.762E-14
	NECP-Atlas(ARC)	1.303E-03	2.107E-04	1.615E + 01	9.293E-15
TENDL-2017	NJOY2016	2.449E-03	4.006E-04	1.560E + 01	1.727E-14
	NECP-Atlas(NRT)	2.449E-03	4.006E-04	1.560E + 01	1.727E-14
	NECP-Atlas(ARC)	1.270E-03	2.067E-04	8.002E + 00	9.110E-15

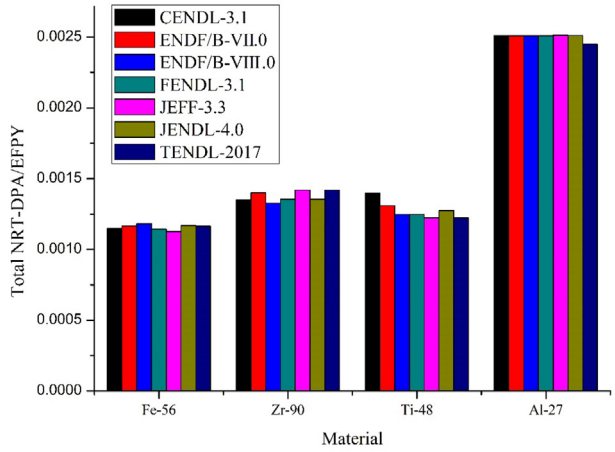

Fig. 30. The total DPA for one EFPY in PWR-RPV.

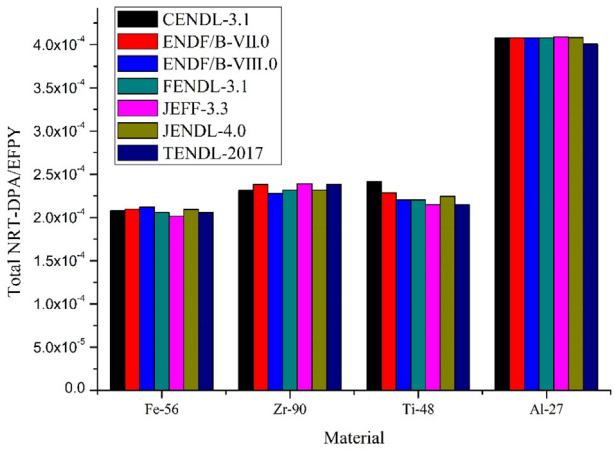

Fig. 31. The total DPA for one EFPY in BWR-RPV.

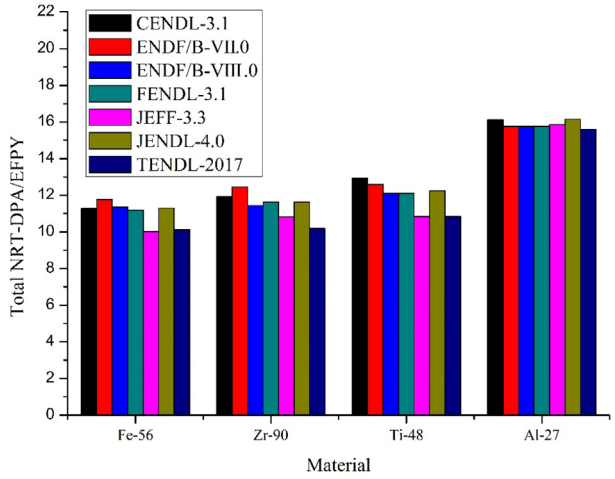

Fig. 32. The total DPA for one EFPY in HCPB-FW -

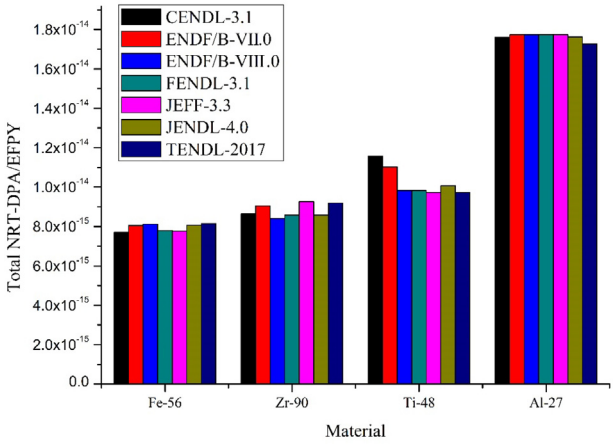

Fig. 33. The total DPA for one EFPY in Superphenix.

istic DPA calculation, the ARC-DPA model is also implemented in NECP-Atlas.

Detailed verification are carried out to ensure the accuracy of the module. The isotopes ^{56}Fe, ^{90}Zr, ^{48}Ti and ^{27}Al are chosen to be calculated. The numerical results show that the heat production and radiation damage energy production cross sections produced by NECP-Atlas agree well with that by NJOY2016. Meanwhile, the heating and DPA in different cases calculated using the cross sections produced by NECP-Atlas also agree well that calculated using the cross sections produced by NJOY2016. A conclusion can be got from the comparison of heating and DPA that the difference between different evaluated nuclear data libraries is very large. Another conclusion is that the DPA calculated using ARC-DPA model is much less than that using NRT-DPA model.

CRediT authorship contribution statement

Wen Yin: Conceptualization, Methodology, Software, Validation, Writing - original draft, Writing - review & editing, Data curation, Visualization. **Tiejun Zu:** Conceptualization, Writing - review & editing, Supervision. **Liangzhi Cao:** Supervision. **Hongchun Wu:** Supervision.

Declaration of Competing Interest

The authors declare that they have no known competing financial interests or personal relationships that could have appeared to influence the work reported in this paper.

Acknowledgements

This research was supported by the National Key R&D Program of China (No. 2017YFE0302200), National Natural Science Foundation of China (No. 11735011) and Fundamental Research Funds for the Central University (No. xzd012019027).

Appendix A. Supplementary data

Supplementary data to this article can be found online at https://doi.org/10.1016/j.anucene.2020.107544.

References

Abdou, M.A., Maynard, C.W., 1975. Calculational methods for nuclear heating-part I: theoretical and computational algorithms. Nucl. Sci. Eng. 56, 360–380.
Bacon, D.J., Gao, F., et al., 2000. The primary damage state in fcc, bcc and hcp metals as seen in molecular dynamics simulations. J. Nucl. Mater. 276, 1–12.
Chen, S., Bernard, D., 2019. Relativistic effect on two-body reaction inducing atomic displacement. J. Nucl. Mater. 522, 236–245.
Chen, S., Bernard, D., Buiron, L., 2019a. Study on the self-shielding and temperature influences on the neutron irradiation damage calculations in reactors. Nucl. Eng. Des. 346, 85–96.
Chen, S., Bernard, D., Tamagno, P., et al., 2019b. Calculation and verification of neutron irradiation damage with differential cross sections. Nucl. Instrum. Methods Phys. Res. Sect. B Beam Interact. Mater. At. 456, 120–132.
Conlin, J.L., et al., 2016. Open Source Release of NJOY2016 and NJOY21. https://njoy.github.io/NJOY2016.
Farawila, Y.M., 1987. Improved Models and Results for Evaluating Neutron Kerma Factors, Ph.D. Dissertation, University of Wisconsin.
Farawila, Y., Gohar, Y., Maynard, C., 1989. KAOS-V code: An evaluation tool for neutron kerma factors and other nuclear responses. Argonne National Laboratory report. ANL/FPP/TM-240.
Fleming, M., et al., 2019. http://fispact.ukaea.uk/wiki/Reference_input_spectra.
Kahler, A.C., MacFarlane, R.E., et al., 2018. The NJOY Nuclear Data Processing System, Version 2016. Los Alamos National Laboratory report. LA-UR-17-20093.
Kinchin, G.H., Pease, R.S., 1955. The displacement of atoms in solids by radiation. Rep. Prog. Phys. 18 (1), 77–86.
Konobeyev, A.Y., Fischer, U., et al., 2017. Evaluation of effective threshold displacement energies and other data required for the calculation of advanced atomic displacement cross-sections. Nucl. Eng. Technol. 3 (3), 169–175.
Lindhard, J., Nielsen, V., et al., 1963. Integral equations governing radiation effects. Mat. Fys. Medd. Dan. Vid. Selsk. 33, 1–42.
MacFarlane, R.E. et al., 2018. The NJOY Nuclear Data Processing System, Version 2016. Los Alamos National Laboratory report. LA-UR-17-20093.
Muir, D.W., 1976. Gamma Rays, Q-Values, and Kerma Factors, Los Alamos Scientific Laboratory report LA-6258-MS.
Nordlund, K., Zinkle, S.J., et al., 2018. Improving atomic displacement and replacement calculations with physically realistic damage models. Nat. Commun. 9 (1), 173–191.
Norgett, M.J., Robinson, M.T., Torrens, I.M., 1975. A proposed method of calculating displacement dose rates. Nucl. Eng. Des. 33 (1), 50–54.
Ritts, J., Solomite, M., Stevens, P., 1969. Calculations of neutron fluence-to-kerma factors for the human body. Nucl. Applic. Tech. 7 (1), 89–99.
Robinson, M.T., 1970. Energy dependence of neutron radiation damage in solids. Oak Ridge National Lab, Tenn.
Robinson, M.T., Torrens, I.M., 1974. Computer simulation of atomic-displacement cascades in solids in the binary-collision approximation. Phys. Rev. B 9 (12), 5008–5024.
Wooding, S.J., Howe, L.M., et al., 1998. A molecular dynamics study of high-energy displacement cascades in α-zirconium. J. Nucl. Mater. 254, 191–204.
Zhang, L., Abdou, M.A., 1997. Kerma factor evaluation and its application in nuclear heating experiment analysis. Fusion. Eng. Des. 36, 479–503.
Zinkle, S.J., Singh, B.N., 1993. Analysis of displacement damage and defect production under cascade damage conditions. J. Nucl. Mater. 199, 173–191.
Zu, T., Xu, J., et al., 2019. NECP-Atlas: A new nuclear data processing code. Ann. Nucl. Eng. 123, 153–161.